*Proceedings of the International Conference on Industrial Engineering and Operations Management*

Publisher: IEOM Society International, USA DOI: 10.46254/NA11.20260263
Published: June 9, 2026

# Temporal Interference Neurostimulation for Atypical Trigeminal Neuralgia: A Sensor-Driven Data-Enhanced Approach

**Bishop Egwe, Oluwaseun O Tooki and Aduramigba Lazarus**
Electrical and Electronic Engineering Department
University of Ibadan
Ibadan, Nigeria
begwe425@stu.ui.edu.ng, tooki.oluwaseun@ieee.org, alazarus437@stu.edu.ng

**Olawale Popoola**
Professor
Centre for Energy and Electric Power (CEEP)
Electrical Engineering Department
Tshwane University of Technology
Pretoria, South Africa
PopoolaO@tut.ac.za

## Abstract

Atypical Trigeminal Neuralgia (ATN) represents a debilitating, refractory chronic pain condition often resistant to pharmacological management, necessitating deep-brain stimulation techniques that traditionally require invasive neurosurgical leads. To address the critical need for non-invasive, timely intervention, this study utilized the SIMNIBS 4.5 finite element analysis pipeline to computationally validate Temporal interference (TI) stimulation as the actuator stage for a proposed novel sensor-driven, closed-loop neuromodulation system. Using a high-resolution anatomical head phantom, the authors modelled a specialized infraorbital-occipital electrode montage designed to geometrically steer the interference envelope to the skull base. The simulation applied a 2 kHz and 2.005 kHz carrier frequency paradigm to generate a computationally demonstrated therapeutic 5 Hz beat at the Trigeminal Ganglion (TG) integrated within a theoretical control framework proposed to be triggered by physiological biomarkers of pain, including Heart Rate Variability (HRV) and Electrodermal Activity (EDA). Results demonstrated a successful focal intersection at the petrous apex, achieving a suprathreshold TI envelope magnitude of 0.36V/m within the target ganglion while minimizing superficial cortical exposure. Furthermore, safety analysis confirmed a peak Specific Absorption Rate (SAR) of 0.14W/Kg, significantly below the 2.0W/Kg over a 10-g cubic volume ICNIRP limit. These findings computational validate the biophysical feasibility of TI to non- invasively engage deep cranial nerves, supporting the development of responsive, closed-loop computationally demonstrated therapeutic architectures for refractory ATN.

## Keywords
Atypical Trigeminal Neuralgia, Temporal Interference, Neurostimulation and Trigeminal Neuralgia

## 1. Introduction

### 1.1. Atypical Trigeminal Neuralgia

Trigeminal neuralgia (TN) is a chronic neuropathic pain disorder marked by abrupt, intense, electric-shock-like facial pain episodes along one or more trigeminal nerve branches (IHS Classification of Disorders, 3rd edition). This chronic

pain stems from peripheral trigeminal nerve injury or inflammation (Rana et al. 2023). Atypical trigeminal neuralgia (ATN), also referred to as type 2 TN, is characterized by a constant, aching, burning, or throbbing facial pain rather than the brief electric-shock–like paroxysms typical of classic TN (Zarkrwzeska and Linskey, 2015). Treating ATN is challenging, as patients often fail to respond to first-line drugs like carbamazepine or stop due to side effects (Di Stefano et. al. 2021). Surgical outcomes for ATN are significantly poorer than classic TN (Tyler-Kabara et al. 2002). Potential mechanisms of ATN involve peripheral and central nociceptive circuit dysfunctions, with neurostimulation inducing adaptive reorganization to resolve these dysfunctions (Rana et al. 2023). Some invasive neurostimulation methods exist; however, many patients would prefer non-invasive management methods.

Previous clinical trials exploring non-invasive management of TN have yielded mixed results; for instance, Connell et. al. (2021). Non-invasive deep-targeted stimulation methods, such as Temporal Interference (TI) stimulation, have been proposed as promising alternatives (Grossman et. al. 2017). However, the highly variable and episodic nature of ATN pain requires a treatment modality that can be initiated rapidly upon pain onset to maximize efficacy and minimize overall stimulation duration. We therefore propose a sensor-driven, closed-loop TI framework.

### 1.2. Principles of Temporal Interference (TI) Stimulation

TI works by applying two high-frequency sinusoidal electric fields with slightly different frequencies, whose interaction produces a low-frequency amplitude-modulated envelope at depth (Grossman et al. 2017). If the applied electric fields have frequencies $f_1$ and $f_2$ (where $f_1 \approx f_2$), the resulting electric field at any point can be modeled as the superposition:

$$E(t) = E_1 \sin(2\pi f_1 t) + E_2 \sin(2\pi f_2 t) \qquad (1)$$

Assuming the electric field vectors $E_1$ *and* $E_2$ are co-linear at the interference locus, and using trigonometric identities, this becomes an amplitude modulated signal:

$$E(t) \approx 2E_0 \cos\left(2\pi \frac{f_2 - f_1}{2} t\right) \sin\left(2\pi \frac{f_2 + f_1}{2} t\right) \qquad (2)$$

which consists of a high-frequency carrier at the average frequency $f_{carrier} = \frac{f_1 + f_2}{2}$ and a low-frequency envelope at the difference (or beat) frequency $f_{env} = |f_2 - f_1|$ (Grossman et. al., 2017). When these currents intersect within neural tissue, they produce a low-frequency envelope at the interference locus, capable of driving neuronal firing without stimulating overlying tissue (Grossman et. al., 2017).

The primary advantage of TI is its ability to target deep brain structures while minimizing electric field exposure at superficial layers, reducing off-target effects and discomfort (Grossman et al. 2017; Rampersad et al. 2019). While foundational studies have validated the efficacy of TI in rodents (Grossman et. al. 2017), human applications face challenges like skull resistivity shunting currents (Datta et. al., 2012), requiring optimized electrode montages. Recent modeling work further supports the feasibility of TI for selective deep stimulation in humans (Rampersad et al. 2019). Recent human hippocampal and clinical pilot studies (Perderson et. al; Yang et. al) also support TI's translational potential, however its application to cranial nerve targets such as the trigeminal ganglion remains unexplored

Recent human studies have begun translating TI from computational and animal models into clinical feasibility. Violante et al. (2023) provided the first direct evidence of non-invasive TI targeting the human hippocampus, demonstrating steerable modulation of deep brain activity with minimal cortical exposure using fMRI and behavioral measures of episodic memory enhancement. This landmark study confirmed that TI can focally engage deep structures in humans, supporting the biophysical principles applied in the present work. Subsequent studies have extended these findings: Missey et al. (2024) applied TI to the hippocampus in patients with mesiotemporal lobe epilepsy and observed significant suppression of interictal epileptiform discharges and pathological high-frequency oscillations via intracranial recordings (Pederson et al 2024). Yang et al. (2024) reported preliminary clinical benefits in mild Parkinson's disease, with a single session of TI targeting the globus pallidus improving motor symptoms such as bradykinesia and tremor. Systematic reviews and additional trials (e.g., Demchenko et al, 2025) further indicate that transcranial TI stimulation is generally safe and well-tolerated across motor cortex, basal ganglia, and hippocampal targets in over 20 human studies to date.

These emerging human data reinforce the promise of TI for cranial nerve and deep-brain targets like the trigeminal ganglion, while also highlighting challenges such as inter-subject anatomical variability and the need for individualized montages—issues directly addressed through our high-resolution SimNIBS modeling.

## 2. Rationale For Computational Modelling and Closed-Loop Intervention

### 2.1. Justification for Finite Element Method (FEM) Simulation

Deep-brain stimulation (DBS) montages are inherently limited by the head's inhomogeneous conductivity. The skull, possessing a conductivity about 20–50 times lower than soft tissue, shunts the majority of applied current across the scalp rather than into the brain (Datta et. al. 2012).

Finite Element Method (FEM) modeling is therefore essential for preclinical planning of Temporal Interference (TI) stimulation. It enables accurate simulation of current flow through the highly inhomogeneous tissues of the head, precisely capturing the complex cortical and skull-base geometry that is critical for deep targeting. Small anatomical variations — such as differences in skull thickness, conductivity, or petrous apex morphology — can substantially shift the location and intensity of the TI interference envelope, potentially causing the stimulation focus to miss deep targets such as the trigeminal ganglion (Rampersad et. al. 2019). Computational validation is therefore required to ensure safe and accurate target engagement in human studies.

### 2.2. Necessity for Closed-Loop Control

Modeling solves spatial targeting, but timing requires closed-loop control. ATN is characterized by changing pain states rather than a static baseline. Open-loop systems suffer from two major deficits: (1) unnecessary energy delivery during pain-free periods, reducing battery life in wearable devices (Little. et. al. 2013). (2) the risk of neural habituation (tolerance), where the therapeutic efficacy reduces over time due to homeostatic plasticity (Patil et. al. 2024). Sensor feedback enables on-demand therapy; FEM simulations act as the 'Plant Model,' defining the transfer function from input current to nerve electric field.

### 2.3. Justification for Target Selection

The TG is a sensory ganglion of the trigeminal nerve located in Meckel's cave, containing the cell bodies of primary sensory neurons that convey facial somatosensory and nociceptive information (Cruccu et. al. 2010). TG neurons relay ophthalmic, maxillary, and mandibular inputs to brainstem targets, notably the principal sensory and spinal nuclei (Sessle et. al. 2000). These neurons are central to trigeminal pain processing, transmitting both pain intensity and localization, with hyperexcitability or abnormal firing strongly associated with neuropathic facial pain, including TN and ATN (Denvor et. al. 2002). The TG is a preferred target in trigeminal pain neuromodulation due to its accessibility and critical role in interrupting aberrant nociceptive signaling before it reaches central structures (Cruccu et. al. 2010).

## 3. Study Hypothesis and Objectives

Addressing refractory ATN, we hypothesize a 2-channel non-invasive, TI montage targeting the TG that focuses simulated therapeutic fields deeply while sparing superficial tissue. Using SimNIBS, we aim to:

i. Optimize placement and parameters for maximal TG intensity;
ii. Quantify spatial selectivity (target-to-cortex ratio); and
iii. Confirm safety compliance (Specific Absorption Rate (SAR), peak fields) per international standards.

## 4. Materials And Methods

### 4.1. Computational Modeling Environment

All electric-field simulations were conducted using SimNIBS v4.5. The simulations incorporated the Ernie Extended head model, a high-resolution anatomical phantom (SimNIBS 4.5.0 Release Notes, 2024).

### 4.2. Temporal Interference (TI) Electrode Montage Design

Conventional transcranial direct current stimulation (tDCS) montages were evaluated and deemed unsuitable for deep trigeminal targeting; hence, the proposed **Infraorbital-Occipital** montage was developed. We modeled 20mm elliptical cheek electrodes and 50mm rectangular occipital pads, assuming ideal scalp contact and electrodes were modeled with the conductivity of standard saline-soaked sponge material ($\sigma = 1.4S/\text{mS/m}$) (Saturnino G.B. et. al. 2015; Miranda et. al. 2006).

#### 4.2.1. Electrode Montage and Configuration

The custom montage targeting the petrous apex TG maximizes deep field intersection, unlike standard cortical setups. The four-channel montage was arranged in a contralateral trajectory with two channels: *a)* Anode positioned at the left infraorbital region, cathode positioned at the right occipital (O2) region (International 10-10 System), and *b)* Anode positioned at the right infraorbital region, cathode positioned at the left occipital (O1) region.

This configuration creates an anterior-inferior to posterior-superior current flow, forcing the electric fields to intersect medially at the level of Meckel's cave.

#### 4.2.2. Current Parameters and Waveforms

The TI stimulation was simulated by applying two distinct high-frequency sinusoidal currents. The stimulation parameters were defined based on (Grossman et. al. 2017):

- Carrier Frequencies: Channel 1 was assigned a carrier frequency of $f_1 = 2000Hz$ and Channel 2 was assigned a carrier frequency of $f_2 = 2005Hz$. These frequencies are sufficiently high to bypass neuronal membrane capacitance and minimize direct surface stimulation (Grossman et. al. 2017).

- Beat Frequency: The superposition of the two carrier signals generated an amplitude-modulated envelope oscillating at a beat frequency of $\Delta f = |f_1 - f_2|\ Hz$.

- Current Amplitudes: The injected current intensity for both channels $I_1 = I_2 = 1.0\ mA$. Equal amplitudes were maintained to ensure a modulation depth of 100% at the point of maximal field intersection.

### 4.3. Closed-Loop System Architecture and Trigger Model

We conceptually define the proposed closed-loop architecture and the assumed trigger mechanism.

#### 4.3.1. System Components and Signal Input

The proposed system consists of three main stages: the Sensor/Input Stage, the Processing/Decision Stage, and the Actuator/Output Stage (validated by subsequent SimNIBS Finite Element Analysis (FEA)). For the Sensor/Input Stage, we propose using commercially available wearable sensors to monitor physiological markers linked to autonomic nervous system (ANS) activity and pain. The primary bio signals considered for the trigger are:

- Heart Rate Variability (HRV)**:** Decreased HRV (specifically, lower High-Frequency Power) is associated with elevated stress, pain, and sympathetic nervous system activation, often preceding a pain episode (Koenig et. al. 2013; Forte et. al. 2022).

- Skin Conductance (SC/GSR)**:** Increased Galvanic Skin Response is a marker of sympathetic arousal and emotional distress correlated with subjective pain intensity (Miranda et. al. 2006; Loggia; 2011; Storm 2008).

- Electromyography (EMG): Electromyography (EMG) can be used as an indirect indicator of pain intensity by measuring muscle activity. In craniofacial neuropathies, pain activates a brainstem muscle-guarding reflex, observed in surface EMG as increased baseline activity in the masseter and temporalis during persistent pain, while paroxysmal attacks produce brief high-amplitude bursts, enabling EMG to capture both sustained and transient pain states (Lund J.P. et. al. 1991; Svensson and Graven-Nielson 2001; Cruccu et. al 2016).

#### 4.3.2. Trigger Logic Model

The Processing/Decision Stage would employ a threshold-based logic to initiate TI stimulation. The proposed system would monitor the defined bio signals in real-time. A stimulation session would be triggered when a composite score (CS) derived from these bio signals exceeds a defined clinical threshold $T_{stim}$ for a sustained period of $\tau_{hold}$ (e.g., 30 seconds).

$$Trigger = \begin{cases} TI\ ON & if \quad CS > T_{stim}\ for\ \tau_{hold} \\ TI\ OFF & otherwise \end{cases} \tag{3}$$

The sensor fusion would employ a CS based on normalized (0-1), weighted signals. These results would then validate the theoretical system's output.

### 4.4. Simulation Procedure and Metrics

#### 4.4.1. Finite Element Analysis (FEA) Implementation

The numerical solution for the electric field distribution was computed using the Finite Element Method (FEM) within the SimNIBS v4.5 pipeline (Thielscher et. al. 2015).

The electric potential ($\phi$) was solved using the quasi-static Laplace equation:

$$\nabla \cdot (\sigma \nabla \phi) = 0 \qquad (4)$$

Where $\sigma$ is the frequency-dependent conductivity tensor and $\nabla\phi$ is the electric field.

Boundary conditions were applied as explained in [28].

#### 4.4.2. Calculation of Electric Fields

The electric fields generated by the two electrode pairs were calculated independently. For each channel $k \; \forall \; k \in \{1,2\}$, the electric field, $\vec{E}_k$, at $\vec{r}$ was computed as the negative gradient of the electric potential: $\vec{E}_k = -\nabla\phi_k(\vec{r})$.

#### 4.4.3. TI Electric Field Calculation

The TI effect arises from the superposition of the two time-varying sinusoidal fields ( $\vec{E}_1$ *and* $\vec{E}_2$ ) with slightly differing frequencies ($f_1$ *and* $f_2$). The resulting total electric field is amplitude-modulated at the beat frequency $\Delta f = |f_1 - f_2|$.

The maximal amplitude envelope, denoted as $\vec{E}_{env}$ is calculated mathematically as defined by (Grossman et. al. 2017):

$$|\vec{E}_{env}(\vec{n},\vec{r})| = \left|\left(\vec{E}_1(\vec{r}) + \vec{E}_2(\vec{r})\right).\vec{n}\right| - \left|\left(\vec{E}_1(\vec{r}) - \vec{E}_2(\vec{r})\right).\vec{n}\right| \quad (5)$$

#### 4.4.4. Targeting Metrics and Evaluation

To evaluate the efficacy and safety of the proposed montage, three key quantitative metrics were extracted from the simulation results:

**i. Focal Strength ($\mathbf{E_{TG,max}}$)**

The maximal electric field magnitude reaching the target structure (the TG) was quantified to ensure it met the theoretical threshold for neural activation ($0.2\,\frac{V}{m}$)

$$E_{TG,max} = \max\left(\vec{E}_{env}\right) within\ the\ TG\ ROI \qquad (6)$$

**ii. Selectivity Index:**

To assess the capability of the montage to spare superficial tissue while targeting the deep ganglion, a selectivity ratio was calculated. This metric compares the peak field strength at the target to the peak field strength in the overlaying cortex.

$$Selectivity = \frac{E_{TG,max}}{E_{cortex,max}} \qquad (7)$$

A higher ratio indicates superior deep targeting with reduced off-target superficial stimulation.

From neuroimaging literature, the trigeminal ganglion / Meckel's cave region generally falls within the following approximate MNI coordinates: x = ±20 to ±30 (lateral), y = −18 to −28 (posterior), z = −16 to −24 (inferior) (Borsook et al., 2003). Converting the MNI coordinates to Ernie space coordinates as explained in the SimNIBS documentation, the TG ROI defined (SimNIBS Documentation).

### 4.5. Safety Analysis and IEEE/ICNIRP Compliance

#### 4.5.1. Specific Absorption Rate (SAR) Calculation

To evaluate thermal safety and potential tissue heating, the Specific Absorption Rate (SAR) was derived from the simulated electric field distribution. SAR quantifies the rate at which energy is absorbed per unit mass of biological tissue and is defined by the relationship:

$$SAR(\vec{r}) = \frac{\sigma(\vec{r})|\vec{E}_{total}(\overrightarrow{r})|^2}{2\rho(\overrightarrow{r})} \qquad (8)$$

Where:$\sigma(\vec{r})$ represents the electrical conductivity of the tissue ($S/m$), $|\vec{E}_{total}(\overrightarrow{r})|$ is the peak magnitude of the total electric field ($V/m$) and $\rho(\overrightarrow{r})$ is the mass density of the tissue, approximated as $1{,}050\ kg/m^3$ for cranial tissues (Hasgall et. al. 2012).

Because the simulation employed the quasi-static approximation, the SAR distribution was calculated post-hoc for the worst-case scenario.

#### 4.5.2. Compliance with Safety Standards

The calculated exposure metrics were benchmarked against the international safety guidelines established by the International Commission on Non-Ionizing Radiation Protection (ICNIRP) and the IEEE International Committee on Electromagnetic Safety.

**a) Peak Spatial-Average SAR (psSAR)**

For the applied current intensity of 1.0 $mA$ per channel (2.0 $mA$ total injected current), the maximum localized electric field at the electrode-skin interface was approximately $20 - 25\ V/m$. Based on the conductivity of the scalp ($\sigma = 0.465\ S/m$), the estimated peak local SAR is:

$$SAR_{peak} \approx \frac{0.465 \cdot (25)^2}{2 \cdot 1050} \approx 0.14 W/kg$$

This value is well below the general public safety limit defined by the ICNIRP Guidelines, which cap localized SAR (head and trunk) at 2.0 $W/kg$ averaged over 10 $grams$ of tissue (ICNIRP 1998). Hence, the simulation confirms that the thermal effects of the TI montage are negligible.

## 5. Results

### 5.1. Visualization of TI Electric Field Distribution

The optimized TI montage was evaluated by analyzing the spatial distribution of the envelope of the electric field($|\vec{E}_{env}|$).

#### 5.1.1. Electrode Placement:

**Figure 1** illustrates the four-channel montage placement on the Ernie Extended head model.

#### 5.1.2. Anatomical Slices of E-field Distribution:

**Figure 2** presents superior, lateral, anterior, inferior and posterior views of the brain showing the TI envelope E-field magnitude($|\vec{E}_{env}|$), overlaid onto the anatomical phantom.

High-magnitude field spread outside the target region was minimal. The proposed infraorbital-occipital cross-montage steered the TI envelope to the skull base, achieving a suprathreshold focal intensity of 0.36 $V/m$ within the anatomical region of the TG.

Collectively, the electric field distribution confirms that the infraorbital-occipital montage effectively concentrates the TI envelope at the petrous apex, achieving suprathreshold field strengths ($> 0.2$ V/m) within the TG despite the resistive attenuation of the skull base.

### 5.2. Quantitative Analysis of Targeting Efficacy

#### 5.2.1 Coordinate Reporting

The maximal deep-brain electric field intensity (Hotspot) was localized to the anatomical region of Meckel's Cave.
Ernie Space Coordinates: $x = 21.5, y = -16.4, z = -24.1$.
MNI Coordinates (Approx): $x = \pm 24, y = -22, z = -18$.
The maximal deep-brain electric field intensity (Hotspot) was localized to the anatomical region of Meckel's Cave.

#### 5.2.2. Regional Field Strength Table

Table 1. Peak TI Envelope magnitudes ($E_{env,max}$) across the target and non-target anatomical structures.

| **Anatomical Structure** | **Tissue Type** | $\boldsymbol{E_{env,max}}$ $\boldsymbol{(V/m)}$ | **Activation Interpretation** |
|---|---|---|---|
| Trigeminal Ganglion (Target) | Deep Grey Matter | 0.36 | Suprathreshold ($> 0.2 V/m$) |
| Brainstem (Pons) | Deep White Matter | 0.24 | Threshold ($\sim 0.2 V/m$) |

| | | | |
|---|---|---|---|
| Inferior Temporal Gyrus | Superficial Cortex | 0.92 | Off-Target Hotspot |
| Scalp (Under Electrode) | Skin | 24.15 | Safety Limit (Thermal) |
| Whole Brain Average | Global | 0.11 | Subthreshold ($< 0.2V/m$) |

[ft] *Note: The Target value of 0.36 V/m corresponds to the "Yellow/Green" color seen* in Figure 2. *The 0.92V/m value corresponds to the "Red" spots on the sides.*

Table 1 summarizes the peak TI envelope electric field magnitudes ($E_{env,max}$) across key anatomical structures in the simulated head model, highlighting the targeting efficacy and safety of the proposed montage. The simulation confirmed that this geometric configuration delivers suprathreshold electric fields ($E_{env} > 0.2\,V/m$) to the deep target anatomy (the TG) and threshold electric fields ($\sim 0.2V/m$) to the brainstem. The electric field due to the effect of the envelope on the skin under the electrode was under the thermal safety limit.

### 5.3. TI Selectivity Analysis

#### 5.3.1. Scalp -To - Target Selectivity (Safety Ratio)

This ratio measures the efficiency of delivering current through the resistive skull barrier.

$$Selectivity_{Scalp} = \frac{E_{Target,max}}{E_{Scalp,max}} = \frac{0.36\,V/m}{24.15\,V/m} \approx 0.015$$

#### 5.3.2. Deep - To - Superficial Brain Selectivity (Focus Ratio)

This ratio measures the ability of TI to target deep structures relative to the overlaying cortex.

$$Selectivity_{Brain} = \frac{E_{Target,max}}{E_{Cortex,max}} = \frac{0.36\,V/m}{0.92\,V/m} \approx 0.39$$

Here, we can infer that the TI montage achieves deep focusing, with the electric field at the TG reaching 39% of the cortical peak, while still exceeding the neural activation threshold despite higher superficial fields.

## 6. Discussion

### 6.1. Interpretation of Key Findings and Closed-Loop Implications

#### 6.1.1. Significance of Selectivity Index

The simulation results yielded a Deep -To- Superficial Selectivity Ratio of 0.39 ($\frac{E_{Target}}{E_{Cortex}}$). This metric highlights an advantage of the proposed Infraorbital-Occipital TI montage over conventional tES methods. In bipolar tDCS targeting the skull base, scalp and cerebrospinal fluid (CSF) attenuation reduces selectivity ratios below 0.2, often requiring unsafe skin current densities for effective deep stimulation. This is consistent with existing literature. (Datta et. al. 2009).

Using the geometric steering properties of TI, the proposed montage successfully concentrated the interference envelope at the TG. Despite superficial exposure (0.92 V/m), neuronal membranes filter the 2kHz carrier, rendering it ineffective compared to the low-frequency envelope. (Grossman et. al. 2017).

Therefore, despite the lower selectivity compared to invasive DBS, the selectivity of the TI envelope is superior to standard low-frequency tACS (transcranial Alternating Current Stimulation) applied at the same location.

#### 6.1.2. Validation of The Output Stage (Actuator)

The simulation results confirmed that a total injected current of 2.0 $mA$(1.0$mA$ *per channel*) is sufficient to generate a peak TI envelope magnitude of approximately **0.36 V/m** within the anatomical volume of the TG. This induced field strength exceeds the empirical neural activation threshold of 0.2 $V/m$ (Reato et. al. 2010), (Voroslakos et. al. 2018). Consequently, these results serve as a computational validation of the closed-loop system's output capabilities.

#### 6.1.3. Comparison to Existing Literature

**i. TI vs Invasive Deep Brain Stimulation (DBS)**

Refractory ATN gold standards are invasive, typically involving MVD or motor cortex stimulation (MCS) via implanted leads (Zakrzewska and Linskey, 2015). These methods carry significant surgical risks, including infection and hemorrhage. The simulation results presented here demonstrate that TI can achieve a peak deep-tissue electric field of **0.36 V/m** at the TG region. This value exceeds the established neural activation threshold of 0.2 V/m (Reato et. al. 2010).

Unlike DBS, this non-invasive TI targets the skull base, offering a low-risk alternative for patients ineligible for surgery.

**ii. TI vs Conventions tES (tDCS & tACS)**

Prior tDCS studies show a lack of deep selectivity, as high skull resistivity shunts ~75% of current through the scalp and CSF layers (Voroslakos M. et. al. 2018). Consequently, while electric field strengths at the electrode-skin interface often exceed 20 V/m, the intensity reaching deep neural targets frequently falls below the 0.2 V/m threshold required to reliably modulate neuronal spiking.

In contrast, our results show a Target Selectivity Ratio of 0.39**,** a marked improvement over conventional tES models. Furthermore, the use of the 2KHz carrier frequencies offers a significant advantage over low-frequency tACS. High-frequency carriers minimize cutaneous receptor activation, reducing the sensation of burning or tingling on the scalp (Guleyupoglu et. al. 2013). This characteristic is critical for the proposed closed-loop system as it allows the stimulator to ramp stimulation up and down in response to pain signals without causing sensory discomfort, thereby enabling "on-demand" background neuromodulation.

### 6.2. Relevance to Atypical Trigeminal Neuralgia (ATN)

Preclinical work by (Grossman et. al. 2017) and human trials (Violante et. al. 2004) focused on the hippocampus and the motor cortex. This study extends the application of TI to the cranial nerve architecture.

This applies to ATN (TN Type 2), defined by constant pain with intensity spikes (Cruccu G. et. al 2016). Static stimulation risks neural adaptation and reduced efficacy. Our validation supports a responsive, closed-loop paradigm that dynamically adjusts amplitude to pain fluctuations. The simulated electric field distribution confirms that the actuation stage can effectively target the TG without significant spillover to the brainstem respiratory centers, a crucial safety requirement for automated home-use devices.

### 6.3. Study Limitations

#### 6.3.1. Finite Element Model Simplifications

The simulation relies on inherent simplifications characteristic of FEM modeling. First, the tissue compartments were assigned conductivity values. In reality, biological tissues-like the skull and white matter tracts—exhibit significant anisotropy (Wolters C.H. et. al. 2005). The omission of skull anisotropy may result in a slight overestimation of deep-tissue field strength.

Modeling assumed ideal contact, ignoring hair or sweat. Real-world conditions may increase scalp shunting, necessitating higher currents to achieve target intensities. Goyal et. al. 2022; Gomez-Tames et. al. 2016). The standard ‘Ernie’ Extended head model was used in this study. While this provides a high-resolution and anatomically detailed phantom, it represents only a single individual and therefore neglects the considerable inter-subject anatomical variability inherent in the human population. Variations in skull thickness, bone density, and conductivity could significantly influence current flow paths during transcranial electrical stimulation (Antonakakis M. et. al. 2020). Of particular importance for this work is variability in the geometry of the petrous apex and Meckel’s cave region, including differences in the size and orientation of skull base foramina and the relative position of the trigeminal ganglion. Such anatomical differences can substantially alter local impedance distributions, shift the location of the TI interference envelope, and modify the achieved electric field magnitude at the target. As highlighted by Antonakakis et al. (2020), inter-subject variability in skull conductivity and thickness can lead to notable differences in predicted field distributions, underscoring the need for robust, multi-subject modeling or individualized head models in future translational efforts.

### 6.3.2. Translation of E-Fields to Neural Activation

Quasi-static FEM modeling calculated the physical parameter (Electric Field) and not the biological outcome (Action Potentials). This study utilized the threshold as a proxy for neural activation based on literature standards (Reato et. al. 2010). However, efficacy hinges on electric field alignment with trigeminal root axons. A field perpendicular to a nerve fiber is significantly less effective than a field parallel to it (Rattay, 1986). Therefore, while the simulation confirms that the ($|\vec{E}_{TI}|$) is present at the target, but predicting excitatory or inhibitory responses requires complex multi-scale modeling.

### 6.3.3. Theoretical Nature of The Closed-Loop Sensor Stage

**Alt**hough simulations validate system output, the sensor and trigger models remain theoretical. Linking biosignals to subjective pain is clinically challenging due to artifacts and non-pain arousal, explaining the absence of defined biomarker thresholds. Thus, the architecture is a proof-of-concept requiring in-vivo validation to reliably distinguish ATN pain from noise before full closed-loop implementation. Currently, there is very limited clinical and experimental data on the proposed biomarkers for pain to validate the closed-loop sensor stage. The reliable computation and calibration of the composite score for the proposed trigger mechanism depends heavily on the availability of sufficient high-quality, labeled biomarker data.

### 6.3.4. Future Directions

Clinical translation requires addressing anatomical variability; differences in skull thickness and petrous apex geometry alter impedance paths and shift the TI intersection (Marios A. et. al. , 2020). Future development must quantify montage robustness across diverse MRI datasets and implement personalized protocols for optimized electrode placement.

### 6.3.5. Refinement of The Sensor / Input Stage

System efficacy depends on accurate detection via sensor fusion. We propose a multi-modal ML model (e.g., EEG, autonomic metrics) trained on labeled clinical data. Trigger thresholds must be optimized for sensitivity and specificity to ensure battery efficiency and minimize habituation in wearable devices.

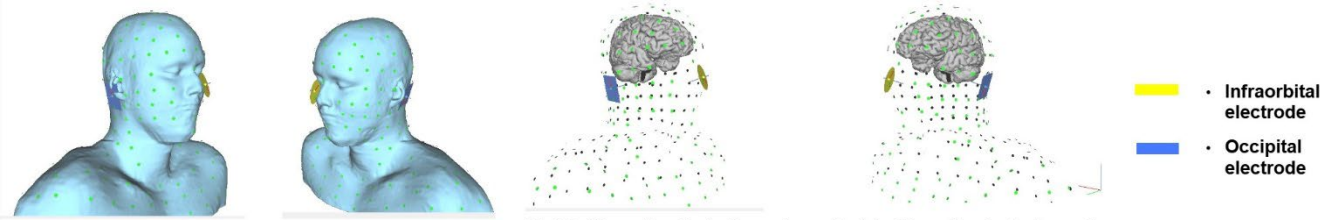


Fig 1.1 - Shows the electrode montage placement for Channel 1 of the infraorbital-occipital montage , with the skin left visible

Fig 1.2 - Shows the electrode montage placement for Channel 2 of the infraorbital-occipital montage , with the skin left visible

Fig 1.3 - Shows the electrode montage placement for Channel 1 of the infraorbital-occipital montage, with the gray metter left visible and skin visibility of the head model disabled.

Fig 1.4 - Shows the electrode montage placement for Channel 2 of the infraorbital-occipital montage, with the gray metter left visible and skin visibility of the head model disabled.

Figure 1. Images showing the Electrode Montage placement on the Ernie Extended Head Model in SIMNIBS v4.5 software with the skin visible and with the grey matter visible. The infraorbital electrodes are in yellow color and the occipital electrodes are in blue. Fig 1.1 and Fig. 1.3 show the electrodes of channel 1 with the skin and grey matter visible respectively and Figure 1.2 and Figure 1.4 show the electrodes of channel 2.

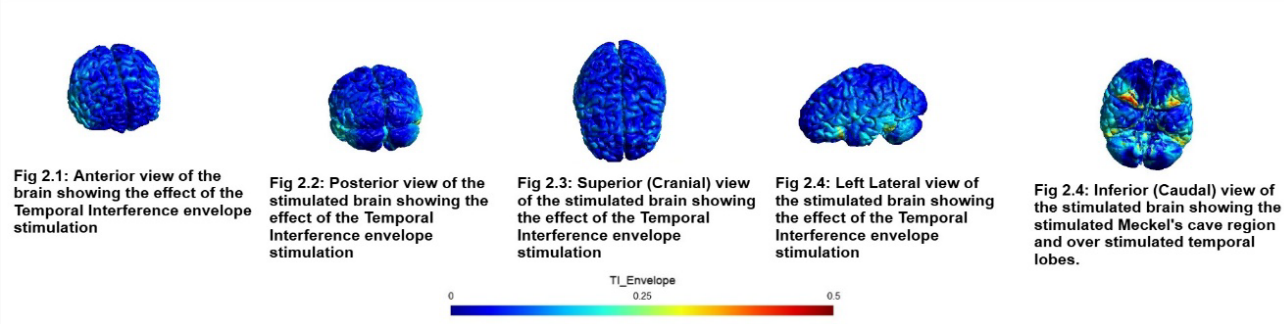


Fig 2.1: Anterior view of the brain showing the effect of the Temporal Interference envelope stimulation

Fig 2.2: Posterior view of the stimulated brain showing the effect of the Temporal Interference envelope stimulation

Fig 2.3: Superior (Cranial) view of the stimulated brain showing the effect of the Temporal Interference envelope stimulation

Fig 2.4: Left Lateral view of the stimulated brain showing the effect of the Temporal Interference envelope stimulation

Fig 2.4: Inferior (Caudal) view of the stimulated brain showing the stimulated Meckel's cave region and over stimulated temporal lobes.

Figure 2. Images of the stimulated brain of the Ernie Extended head model. Here, we see the anterior, posterior, superior, left lateral and inferior views of the stimulated brain, with the color scale depicting the effect of the TI envelope on each part of the brain.

## 7. Conclusion

This study provides a computational validation of a novel non-invasive neuromodulation strategy targeting the TG. Utilizing high-resolution FEM within the SimNIBS v4.5 framework, we demonstrated that a specialized Infraorbital-occipital montage can successfully steer the TI envelope to the skull base. The simulation confirmed that this geometric configuration delivers suprathreshold electric fields $E_{env} > 0.2\ V/m$ to the deep target anatomy while preserving the non-invasive nature of the intervention.

Crucially, these results serve as the engineering verification for the actuator of the proposed closed-loop system. We have established that a realizable injected current of 2.0 mA is sufficient to modulate the trigeminal nerve root, confirming that the hardware specifications are viable for a wearable device. This closed-loop TI architecture combines DBS-like deep targeting with transcutaneous safety, offering a low-risk alternative for refractory chronic craniofacial pain.

## Acknowledgements

This work is based on the research supported wholly/in part by the National Research Foundation of South Africa (Grant Numbers: 150574, KIC 250804351170); and Tshwane University of Technology - Faculty of Engineering and Built Environment and Centre for Energy and Electric Power.

## References

Antonakakis, M., Schrader, S., Aydin, Ü., Khan, A., Gross, J., Zervakis, M., Rampp, S., and Wolters, C. H., "Inter-Subject Variability of Skull Conductivity and Thickness in Calibrated Realistic Head Models," *NeuroImage*, vol. 223, p. 117353, 2020. https://doi.org/10.1016/j.neuroimage.2020.117353.

Baumann, SB., Wozny, DR., Kelly, SK., and Meno, FM., "The electrical conductivity of human cerebrospinal fluid at body temperature," *IEEE Transactions on Biomedical Engineering*, vol. 44, no. 3, pp. 220-223, 1997. https://doi.org/10.1109/10.554770.

Cruccu, G., Bonamico, L. H., and Zakrzewska, J. M., "Cranial neuralgias," *Handbook of Clinical Neurology*, vol. 97, pp. 663-678, 2010. https://doi.org/10.1016/s0072-9752(10)97056-5.

Cruccu, G., et al., "Trigeminal neuralgia," *Neurology*, vol. 87, no. 2, pp. 220-228, 2016. https://doi.org/10.1212/wnl.0000000000002840.

Datta, A., Bansal, V., Diaz, J., Patel, J., Reato, D., and Bikson, M., "Gyri-precise head model of transcranial direct current stimulation: Improved spatial focality using a ring electrode versus conventional rectangular pad," *Brain Stimulation*, vol. 2, no. 4, pp. 201-207, 2009. https://doi.org/10.1016/j.brs.2009.03.005.

Datta, A., Truong, D., Minhas, P., Parra, L. C., and Bikson, M., "Inter-Individual Variation during Transcranial Direct Current Stimulation and Normalization of Dose Using MRI-Derived Computational Models," *Frontiers in Psychiatry*, vol. 3, p. 91, 2012. https://doi.org/10.3389/fpsyt.2012.00091.

Devor, M., Amir, R., and Rappaport, Z. H., "Pathophysiology of Trigeminal Neuralgia: The Ignition Hypothesis," *The Clinical Journal of Pain*, vol. 18, no. 1, pp. 4-13, 2002. https://doi.org/10.1097/00002508-200201000-00002.

Di Stefano, G., De Stefano, G., Leone, C., Di Lionardo, A., Di Pietro, G., Sgro, E., Mollica, C., Cruccu, G., and Truini, A., "Real-world effectiveness and tolerability of carbamazepine and oxcarbazepine in 354 patients with trigeminal neuralgia," *European Journal of Pain*, 2021.

Forte, G., Troisi, G., Pazzaglia, M., Pascalis, V., and Casagrande, M., "Heart Rate Variability and Pain: A Systematic Review," *Brain Sciences*, vol. 12, no. 2, p. 153, 2022.

Gomez-Tames, J., Sugiyama, Y., Laakso, I., Tanaka, S., Koyama, S., Sadato, N., and Hirata, A., "Effect of microscopic modeling of skin in electrical and thermal analysis of transcranial direct current stimulation," *Physics in Medicine and Biology*, vol. 61, no. 24, pp. 8825-8838, 2016. https://doi.org/10.1088/1361-6560/61/24/8825.

Goyal, K., Borkholder, D. A., and Day, W. S., "Dependence of Skin-Electrode Contact Impedance on Material and Skin Hydration," *Sensors (Basel)*, vol. 22, no. 21, p. 8510, 2022. https://doi.org/10.3390/s22218510.

Grossman, N., Bono, D., Dedic, N., Kodandaramaiah, S. B., Rudenko, A., Suk, H. J., Cassara, A. M., Neufeld, E., Kuster, N., Tsai, L. H., Pascual-Leone, A., and Boyden, E. S., "Noninvasive Deep Brain Stimulation via

emporally Interfering Electric Fields," *Cell*, vol. 169, no. 6, pp. 1029-1041, 2017. https://doi.org/10.1016/j.cell.2017.05.024.

Guleyupoglu, B., Schestatsky, P., Edwards, D., Fregni, F., and Bikson, M., "Classification of methods in transcranial Electrical Stimulation (tES) and evolving strategy from historical approaches to contemporary innovations," *Journal of Neuroscience Methods*, vol. 219, no. 2, pp. 297–311, 2013. https://doi.org/10.1016/j.jneumeth.2013.07.016.

Hasgall, P. A., Neufeld, E., Gosselin, M., Klingenbock, A., and Kuster, N., *IT'IS Database for Thermal and Electromagnetic Parameters of Biological Tissues*, IT'IS Foundation, 2012.

Headache Classification Committee of the International Headache Society (IHS), "The International Classification of Headache Disorders, 3rd edition," *Cephalalgia*, vol. 38, no. 1, pp. 1-211, 2018. https://doi.org/10.1177/0333102417738202.

ICNIRP, 1998; IEEE C95.1-2019, "International 10-10 System," *IEEE Standards*, 2019.

Janssen, A. M., et al., "The influence of sulcus width on simulated electric fields induced by transcranial magnetic stimulation," *Physics in Medicine and Biology*, vol. 58, no. 14, pp. 4881-4896, 2013. https://doi.org/10.1088/0031-9155/58/14/4881.

Koenig, J., Jarczok, M. N., Ellis, R. J., Hillecke, T. K., and Thayer, J. F., "Heart rate variability and experimentally induced pain in healthy adults: A systematic review," *European Journal of Pain*, vol. 18, no. 3, pp. 301-314, 2013. https://doi.org/10.1002/j.1532-2149.2013.00379.x.

Lefaucheur, J. P., André-Obadia, N., Antal, A., Ayache, S. S., Baeken, C., Benninger, D. H., et al., "Evidence-based guidelines on the therapeutic use of repetitive transcranial magnetic stimulation (rTMS)," *Clinical Neurophysiology*, vol. 125, no. 11, pp. 2150-2206, 2014.

Little, S., Pogosyan, A., Neal, S., Zavala, B., Zrinzo, L., Hariz, M., et al., "Adaptive deep brain stimulation in advanced Parkinson disease," *Annals of Neurology*, vol. 74, no. 3, pp. 449-457, 2013. https://doi.org/10.1002/ana.23951.

Loggia, M. L., Juneau, M., and Bushnell, C. M., "Autonomic responses to heat pain: Heart rate, skin conductance, and their relation to verbal ratings and stimulus intensity," *Pain*, vol. 152, no. 3, pp. 592-598, 2011. https://doi.org/10.1016/j.pain.2010.11.032.

Lund, J. P., Donga, R., Widmer, C. G., and Stohler, C. S., "The pain-adaptation model: a discussion of the relationship between chronic musculoskeletal pain and motor activity," *Canadian Journal of Physiology and Pharmacology*, vol. 69, no. 5, pp. 683-694, 1991. https://doi.org/10.1139/y91-102.

Miranda, P. C., Lomarev, M., and Hallett, M., "Modeling the current distribution during transcranial direct current stimulation," *Clinical Neurophysiology*, vol. 117, no. 7, pp. 1623-1629, 2006. https://doi.org/10.1016/j.clinph.2006.04.009.

Nurmikko, T. J., and Eldridge, P. R., "Trigeminal neuralgia--pathophysiology, diagnosis and current treatment," *British Journal of Anaesthesia*, vol. 87, no. 1, pp. 117-132, 2001. https://doi.org/10.1093/bja/87.1.117.

Obermann, M., "Treatment options in trigeminal neuralgia," *Therapeutic Advances in Neurological Disorders*, vol. 3, no. 2, pp. 107-115, 2010. https://doi.org/10.1177/1756285609359317.

O'Connell, N. E., Ferraro, M. C., Gibson, W., Rice, A. S., Vase, L., Coyle, D., and Eccleston, C., "Implanted spinal neuromodulation interventions for chronic pain in adults," *Cochrane Database of Systematic Reviews*, vol. 12, no. 12, p. CD013756, 2021. https://doi.org/10.1002/14651858.CD013756.pub2.

Opitz, A., Paulus, W., Will, S., Antunes, A., and Thielscher, A., "Determinants of the electric field during transcranial direct current stimulation," *NeuroImage*, vol. 109, pp. 140-150, 2015. https://doi.org/10.1016/j.neuroimage.2015.01.033.

Patil, A. S., Levasseur, B., and Gupta, M., "Neuromodulation and Habituation: A Literature Review and Conceptional Analysis of Sustaining Therapeutic Efficacy and Mitigating Habituation," *Biomedicines*, vol. 12, no. 5, p. 930, 2024. https://doi.org/10.3390/biomedicines12050930.

Rampersad, S., Roig-Solvas, B., Yarossi, M., Kulkarni, P. P., Santarnecchi, E., Dorval, A. D., and Brooks, H. D., "Prospects for transcranial temporal interference stimulation in humans: A computational study," *NeuroImage*, vol. 202, p. 116124, 2019. https://doi.org/10.1016/j.neuroimage.2019.116124.

Rana, M. H., Khan, A. A. G., Khalid, I., Ishfaq, M., Javali, M. A., Baig, F. A. H., Kota, M. Z., et al., "Therapeutic Approach for Trigeminal Neuralgia: A Systematic Review," *Biomedicines*, 2023.

Rattay, F., "Analysis of Models for External Stimulation of Axons," *IEEE Transactions on Biomedical Engineering*, vol. BME-33, no. 10, pp. 974-977, 1986. https://doi.org/10.1109/tbme.1986.325670.

Reato, D., Rahman, A., Bikson, M., and Parra, L. C., "Low-Intensity Electrical Stimulation Affects Network Dynamics by Modulating Population Rate and Spike Timing," *The Journal of Neuroscience*, vol. 30, no. 45, pp. 15067-15079, 2010. https://doi.org/10.1523/jneurosci.2059-10.2010.

Saturnino, G. B., Antunes, A., and Thielscher, A., "On the importance of electrode parameters for shaping electric field patterns generated by tDCS," *NeuroImage*, vol. 120, pp. 25-35, 2015. https://doi.org/10.1016/j.neuroimage.2015.06.067.

Sessle, B. J., "Acute and Chronic Craniofacial Pain: Brainstem Mechanisms of Nociceptive Transmission and Neuroplasticity, and Their Clinical Correlates," *Critical Reviews in Oral Biology & Medicine*, vol. 11, no. 1, pp. 57-91, 2000. https://doi.org/10.1177/10454411000110010401.

SimNIBS 4.5.0 Release Notes, "Head And Shoulders - The Impact Of An Extended Head Model On The Simulation And Optimization Of Transcranial Electric Stimulation," *Imaging Neuroscience*, 2024. https://doi.org/10.1162/imag_a_00379.

Storm, H., "Changes in skin conductance as a tool to monitor nociceptive stimulation and pain," *Current Opinion in Anaesthesiology*, vol. 21, no. 6, pp. 796-804, 2008. https://doi.org/10.1097/aco.0b013e3283183fe4.

Svensson, P., and Graven-Nielsen, T., "Craniofacial muscle pain: review of mechanisms and clinical manifestations," *Journal of Orofacial Pain*, vol. 15, no. 2, pp. 117-145, 2001.

Thielscher, A., Antunes, A., and Saturnino, G. B., "Field modeling for transcranial magnetic stimulation: A useful tool to understand the physiological effects of TMS?," *2015 37th Annual International Conference of the IEEE EMBC*, pp. 222-225, 2015. https://doi.org/10.1109/embc.2015.7318340.

Thielscher, A., Opitz, A., and Windhoff, M., "Impact of the gyral geometry on the electric field induced by transcranial magnetic stimulation," *NeuroImage*, vol. 54, no. 1, pp. 234-243, 2011. https://doi.org/10.1016/j.neuroimage.2010.07.061.

Tyler-Kabara, E. C., Kassam, B. B., Horowitz, M. H., Urgo, L., Hadjipanayis, C., Levy, E. I., and Chang, Y. F., "Predictors of outcome in surgically managed patients with typical and atypical trigeminal neuralgia: comparison of results following microvascular decompression," *Journal of Neurosurgery*, 2002.

Violante, I. R., Alania, K., Cassarà, A. M., Neufeld, E., Acerbo, E., Carron, R., Williamson, A., Kurtin, D. L., Rhodes, E., Hampshire, A., Kuster, N., Boyden, E. S., Pascual-Leone, A., and Grossman, N., "Non-invasive temporal interference electrical stimulation of the human hippocampus," *Nature Neuroscience*, vol. 26, no. 11, pp. 1994–2004, 2023.

Vöröslakos, M., et al., "Direct effects of transcranial electric stimulation on brain circuits in rats and humans," *Nature Communications*, vol. 9, no. 1, 2018. https://doi.org/10.1038/s41467-018-02928-3.

Wolters, C. H., Anwander, X., Tricoche, X., Weinstein, D., Koch, M. A., and MacLeod, R. S., "Influence of tissue conductivity anisotropy on EEG/MEG field and return current computation in a realistic head model," *NeuroImage*, vol. 30, no. 3, pp. 813-826, 2006. https://doi.org/10.1016/j.neuroimage.2005.10.014.

Zakrzewska, J. M., and Linskey, M. E., "Trigeminal neuralgia," *BMJ*, vol. 350, p. h1238, 2015. https://doi.org/10.1136/bmj.h1238.

## Biographies

**Bishop Egwe** is an undergraduate student of the Electrical and Electronic Engineering Department of the University of Ibadan, Nigeria. He is a student who has shown great interest in research and academia. Coupled with his school curriculum, he has worked on several personal biomedical engineering hardware projects and participated in several student paper contests at the national and international levels. He was a recipient of the IEEE Honorary mention at the IEEE 2025 Eurocon 2025 Conference, where he, alongside his other two teammates, represented the University of Ibadan as Team Dormisense at the IEEEDuino contest. He also participated in the IEEE SSCS 2025 Contest, where he and his team worked on a system for Narcolepsy patients. He is a student who has shown great potential in academia and hopes to pursue a career in the same.

**Oluwaseun Olayinka Tooki** has a Ph.D degree in Electronic and Electrical Engineering from Ladoke Akintola University of Technology (LAUTECH), Ogbomoso, Nigeria. He is a Senior lecturer and researcher at the Electrical and Electronic Engineering Department, University of Ibadan (UI), Ibadan, Nigeria. He is a senior member of IEEE, a registered member of the Council for the Regulation of Engineering in Nigeria. His research interests include Communication Engineering, Artificial Intelligence in Energy, and Security and Privacy in Energy System.

**Aduramigba Lazarus** is an undergraduate student of Electrical and Electronic Engineering at the University of Ibadan. She has demonstrated interest in the intersection of innovative research and industry applications in science and engineering. Besides her ongoing undergraduate studies, she has cumulative nine-month internship experience as a network engineer at Aviat Networks where she supported engineering teams in providing seamless telecommunications services across various applications. She has also worked on hardware projects and participated in various engineering competitions. In addition, Ms. Lazarus is an avid IEEE volunteer and currently serves as WIE

chair at the IEEE University of Ibadan Student Branch. She is also an ambassador for IEEE PES/IAS PAC 2026. She is intentional about research and building innovative engineering solutions.

**Olawale Popoola** is a Full Professor and Director of the Centre for Energy and Electric Power (CEEP) in the Department of Electrical Engineering at Tshwane University of Technology Pretoria, South Africa. He is an Engineer/technologist/lecturer/author with diverse experience in the Electrical and Power industry, Oil and Gas Sector, Shipping Building Industry, Education, Energy and Quality Management field. His love for research and innovation has brought him accolades and achievements. These include a commendation letter from Weatherford Headquarters, Ravenna, Italy at the earliest stage of his career, various institutional awards, a certificate of recognition by the Department of Science and Technology, South Africa in the invention of South African Patent No 2016/04429 as well as grants/project funds. He is a Certified Measurement and Verification Professional (CMVP) with a proven record and extensive knowledge of the energy industry; and a member of the Association of Energy Engineers (AEE). Olawale is an author/co-author of more than 140 scientific publications (articles, chapters in books and author of a book). Prof Popoola currently holds the Sasol/DSI-NRF Research Chair at tier 2 - "Energy Solutions for Inclusive and Sustainable Societies".